

Can Existing Theory Predict the Response of Tropical Cyclone Intensity to Idealized Landfall?

JIE CHEN* AND DANIEL R. CHAVAS

Purdue University, West Lafayette, Indiana

ABSTRACT

Tropical cyclones cause significant inland hazards, including wind damage and freshwater flooding, that depend strongly on how storm intensity evolves at and after landfall. Existing theoretical predictions for the time-dependent and equilibrium response of storm intensity have been tested over the open ocean but not yet to be applied to storms after landfall. Recent work examined the transient response of the tropical cyclone low-level wind field to instantaneous surface roughening or drying in idealized axisymmetric f -plane simulations. Here, experiments testing combined surface roughening and drying with varying magnitudes of each are used to test theoretical predictions for the intensity response. The transient response to combined surface forcings can be reproduced by the product of their individual responses, in line with traditional potential intensity theory. Existing intensification theory is generalized to weakening and found capable of reproducing the time-dependent inland intensity decay. The initial (0-10min) rapid decay of near-surface wind caused by surface roughening is not captured by existing theory but can be reproduced by a simple frictional spin-down model, where the decay rate is a function of surface roughness. Finally, the theory is shown to compare well with the prevailing empirical decay model for real-world storms. Overall, results indicate the potential for existing theory to predict how tropical cyclone intensity evolves after landfall.

1. Introduction

Landfalling tropical cyclones (TCs) bring tremendous damage to both coastal and inland regions (Rappaport 2000, 2014; Villarini et al. 2014). These damages may change in the future should TCs move and/or decay more slowly in a warming climate (Kossin 2018, 2019; Li and Chakraborty 2020). Therefore, a credible estimation of TC intensity decay after landfall is essential for hazard prediction. Having a physically-based theoretical solution for the storm intensity response to landfall could help improve risk assessment, both in real time for impending landfall events and in climatological studies (Jing and Lin 2020; Xi et al. 2020). However, the underlying physics governing this post-landfall response are not well understood, and no such predictive theory currently exists.

Past research has examined TC intensity at and after landfall via numerical simulations of historical cases and statistical models. Numerical models have limited capacity to predict post-landfall intensity due to the difficulty of capturing the physics over complex terrain, which is not necessarily improved by increasing model resolution or assimilating observational data (Shen 2005; Liu et al. 2017). Moreover, site-specific case studies are not read-

ily generalized to a more fundamental understanding of the storm response to landfall over a wide range of land surfaces. An alternative approach is the use of empirical models or probabilistic models to predict storm inland intensity decay, which may incorporate both storm and environmental parameters (Kaplan and DeMaria 1995, 2001; Vickery and Twisdale 1995; Vickery 2005; DeMaria et al. 2006; Bhowmik et al. 2005). Empirical models have been incorporated into the Statistical Hurricane Intensity Prediction Scheme for the Atlantic and eastern Pacific Oceans (DeMaria and Kaplan 1994; DeMaria et al. 2005) and Statistical Typhoon Intensity Prediction Scheme for the western North Pacific (Knaff et al. 2005), and have been tested for landfalling hurricanes along the South China Coast (Wong et al. 2008). Statistical models have also been incorporated into hurricane risk assessment models in the context of climate change (Vickery et al. 2000; Emanuel et al. 2006; Jing and Lin 2020). However, current statistical models do not incorporate the physics of hurricane intensity decay over land, and their accuracy is limited by the data collected to train the model. Thus, empirical models offer limited fundamental understanding of the inland decay of hurricane intensity, particularly under a changing climate.

Physically-based theoretical models are formulated for TCs over the ocean. Quasi-steady state theories for the

*Corresponding author address: Jie Chen, Purdue University, 550 Stadium Mall Dr., West Lafayette, IN 47907.
E-mail: chen2340@purdue.edu

tropical cyclone date back to Lilly and Emanuel (1985, unpublished manuscript), Shutts (1981), Emanuel (1986, hereafter referred to E86). More recently, theory now exists for TC intensification over the ocean (Emanuel (2012), hereafter referred to E12) that was found to compare well with an axisymmetric model simulation (Emanuel 2018). However, due to the complexities in the transition from ocean to land, research has yet to develop a theory for post-landfall decay that account for the basic physics of the response of a tropical cyclone to landfall. Meanwhile, the potential for existing theoretical models for storms over the ocean to be applied after landfall has yet to be explored. Therefore, testing existing theories against idealized landfalls is a natural step to understand how known physics can or cannot explain the response of TC intensity after landfall. This is the focus of our work.

Chen and Chavas (2020, hereafter referred to CC20) idealized landfall as a transient response of a mature axisymmetric TC to instantaneous surface forcing: surface roughening or drying, each over a range of magnitudes. They tested the response to each forcing individually and showed that each ultimately causes the storm to weaken but via different mechanistic pathways. They further showed that the final equilibrium intensity in response to each forcing can be predicted by E86 potential intensity theory. A logical next step is to test whether the transient intensity response can be predicted by existing theory and, further, whether results can be generalized to any combination of surface drying and roughening adjusted simultaneously. Both outcomes would be more directly relevant to a wide range of inland surfaces felt by storms in real-world landfalls.

Therefore, in this work, both steady-state intensity theory (E86) and time-dependent intensity change theory (E12) are tested against different sets of simulations where surface roughness and wetness are individually/simultaneously modified instantaneously beneath a mature axisymmetric tropical cyclone. We seek to answer the following research questions:

1. Can traditional potential intensity theory predict the equilibrium response to simultaneous surface drying and roughening?
2. Can the transient response to simultaneous drying and roughening be predicted from the responses to each forcing individually?
3. Can existing intensification theory predict the transient decay response to surface drying and/or roughening?
4. Do the theories work for the intensity both near the surface and near the top of the boundary layer?

This paper is structured as follows. Section 2 reviews the relevant theories and demonstrates how they may be

applied to predict the intensity response to surface forcings. Section 3 describes our idealized simulation experiments that are used to test the theory. Section 4 presents our results addressing the research questions. Section 5 summarizes key results, limitations, and avenues for future work.

2. Theory

This work examines two existing theories that predict the equilibrium intensity (E86) and the time-dependent intensity change (E12) of a tropical cyclone. The original motivation of such theories is for storms over the ocean. CC20 found that the equilibrium response of a mature TC to instantaneous surface roughening or drying followed the response predicted by E86 theory closely. This work expands on CC20 by testing both the E86 and E12 theory and generalizes the experiments to simultaneous surface roughening and drying. This section reviews each theoretical prediction and demonstrates how they can be formulated to apply to idealized landfall experiments.

a. Equilibrium intensity prediction: E86

Potential intensity is a theoretical upper-bound for the tropical cyclone intensity in a given thermodynamic environment. This theory is formulated by idealizing a mature tropical cyclone as a Carnot heat engine, where entropy fluxes from the ocean surface are used to maintain the circulation against surface frictional dissipation. Potential intensity V_p is expressed as (Bister and Emanuel 1998),

$$V_p = \sqrt{\frac{C_k}{C_d} \eta (\Delta k)} \quad (1)$$

where

$$\eta = \frac{T_{ST} - T_{tpp}}{T_{tpp}} \quad (2)$$

$$\Delta k = C_p(T_{ST} - T_a) + \varepsilon L_v(q^*(T_{ST}) - q_a(T_a)) \quad (3)$$

C_k and C_d are bulk exchange coefficient for surface enthalpy and momentum, respectively; Δk is the difference between the saturation enthalpy of the ocean surface and the enthalpy of the overlying near-surface air; T_{ST} is the surface temperature, T_a is the temperature of air overlying the surface; T_{tpp} is the tropopause temperature; L_v is the enthalpy of vaporization; C_p is the specific heat capacity of air; q^* is the saturation mixing ratio of the ocean surface at the local surface pressure; q_a is the mixing ratio of air overlying the ocean surface; and ε is surface evaporative fraction, which is taken as 1 over ocean surface. This formulation includes the effect of dissipative heating, which results in the tropopause temperature replacing the surface temperature in the denominator of the Carnot efficiency factor (Bister and Emanuel 1998).

For inland storms, where the underlying surface has a higher C_d (i.e., a rougher surface) and smaller ε (i.e., a

drier surface), Eq.(1) would predict a weaker maximum sustained wind speed compared to the ocean environment. Thus, we define the response of V_p to any given surface forcing as the ratio of its post-forcing value to its initial pre-forcing value. Following CC20, the predicted V_p response to surface roughening is given by

$$\tilde{V}_{p(C_d)} = \frac{V_{p(C_d)}}{V_{p(CTRL)}} = \sqrt{\frac{C_d}{(C_d)_{EXP}}} \quad (4)$$

or surface drying given by

$$\tilde{V}_{p(\varepsilon)} = \frac{V_{p(\varepsilon)}}{V_{p(CTRL)}} = \sqrt{\frac{C_p \Delta T + (\varepsilon)_{EXP} L_v \Delta q}{\Delta k}} \quad (5)$$

where $(C_d)_{EXP}$ and $(\varepsilon)_{EXP}$ are the modified value of each respective surface property parameter, representing various magnitudes of surface roughening or drying. $V_{p(CTRL)}$ is the potential intensity of a Control pre-landfall TC (defined in Section 3). As discussed in CC20, using normalized responses of V_p can generalize the results to any mature storm intensity and also minimizes sensitivities associated with the precise definition of V_p . CC20 demonstrated that the final equilibrium intensity response in idealized simulations closely follows this prediction.

Here we expand this approach to simultaneous surface drying and roughening, i.e.

$$\tilde{V}_{p(C_d \varepsilon)} = \frac{V_{p(C_d \varepsilon)}}{V_{pCTRL}} = \frac{\sqrt{\frac{C_k}{(C_d)_{EXP}} \eta (C_p \Delta T + (\varepsilon)_{EXP} L_v \Delta q)}}{\sqrt{\frac{C_k}{C_d} \eta \Delta k}} \quad (6)$$

Mathematically, Eq.(6) indicates that the equilibrium intensity response to simultaneous forcing, $\tilde{V}_{p(C_d \varepsilon)}$, is simply the product of the individual equilibrium responses, $\tilde{V}_{p(C_d)}$ and $\tilde{V}_{p(\varepsilon)}$, i.e.

$$\tilde{V}_{p(C_d \varepsilon)} = \tilde{V}_{p(C_d)} \tilde{V}_{p(\varepsilon)}. \quad (7)$$

The implication is that the response to any combination of surface roughening and drying may be predictable from the responses to each individual forcing. Inspired by Eq.(7), the complete time-dependent response of storm intensity $\tilde{v}_{m(C_d \varepsilon)}(\tau)$ to simultaneous surface roughening and drying is hypothesized as the product of the individual transient responses, i.e.

$$\tilde{v}_{m(C_d \varepsilon)}(\tau) \approx \tilde{v}^*(\tau) = \tilde{v}_{m(C_d)}(\tau) \tilde{v}_{m(\varepsilon)}(\tau) \quad (8)$$

The above outcome would have significant practical benefits for understanding the response to a wide range of surface properties as is found in nature.

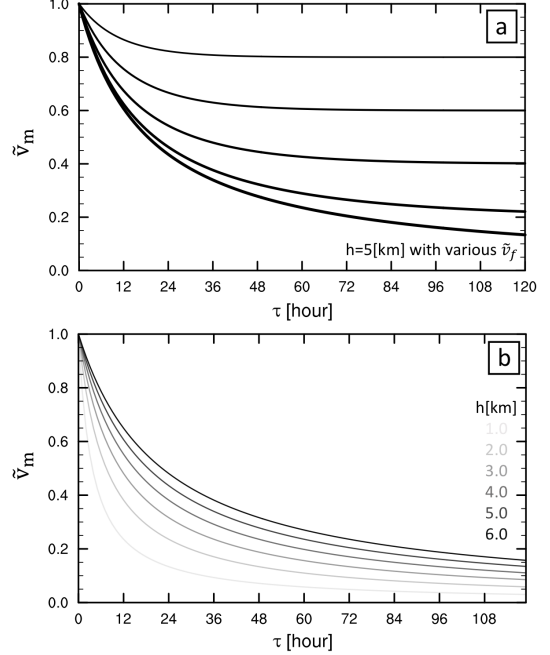


FIG. 1. Normalized intensity decay predicted by E12 theory with $v_m(0) = 100 \text{ ms}^{-1}$: (a) varying \tilde{v}_f with $h = 5 \text{ km}$, for $v_f = 80\%$, 60%, 40%, 20% and 0% of initial intensity (Eq.(10)); (b) varying h with $\tilde{v}_f = 0$ (Eq.(11)). Note that for $\tilde{v}_f = 0$, intensity reaches zero only as $\tau \rightarrow \infty$.

b. Transient intensity prediction: E12

E12 presents a theory for the time-dependent intensification of a TC, based on the role of outflow turbulence in setting the radial distribution of low-level entropy proposed in Emanuel and Rotunno (2011). The equation is given by

$$v_m(\tau) = v_f \tanh\left(\frac{C_k v_f}{2h} \tau\right) \quad (9)$$

with initial condition $v_m = 0$ at $\tau = 0$, where v_{max} is the final steady-state maximum wind speed and h is a constant boundary layer depth scale within the eyewall. Ramsay et al. (2020) generalized this equation to predict intensification from a non-zero initial intensity. Here we further generalize Eq.(9) to represent the decay from an initial intensity $v_m(0)$ to a weaker equilibrium intensity v_f (see Appendix). This can be written in a form normalized by the initial intensity given by

$$\tilde{v}_{m(th)}(\tau) = \tilde{v}_f \coth\left(\frac{C_k v_f}{2h} \tau + \tanh^{-1}(\tilde{v}_f)\right) \quad (10)$$

where $\tilde{v}_{m(th)}(\tau) = \frac{v_{m(th)}(\tau)}{v_m(0)}$ and $\tilde{v}_f = \frac{v_f}{v_m(0)}$. We use the subscript th to denote the intensity predicted by theory. Examples of the theoretical prediction of Eq.(10) are presented in Fig.1a for a range of v_f , using the value of h (5 km) that was applied in E12 and an initial intensity of 100 ms^{-1} .

When $v_f = 0$, Eq.(10) reduces to

$$\tilde{v}_{m(th)}(\tau) = \left(\frac{C_k v_m(0)}{2h} \tau + 1 \right)^{-1} \quad (11)$$

For this special case, the transient intensity response from a given $v_m(0)$ depends only on the boundary layer depth scale h . Fig.1b presents examples varying h over a wide range of values, with using $v_m(0) = 100 \text{ ms}^{-1}$ and $v_f = 0$. Eq. (11) is the continuous limit of Eq.(10) as $v_f \rightarrow 0$ and is not singular. Note that setting $v_f = 0$ produces a solution that does not actually reach zero intensity in finite time, but rather approaches zero only as $\tau \rightarrow \infty$; for realistic timescales, the solution still predicts a normalized intensity appreciably greater than zero ($\approx 15\%$ after 5 days in Fig.1).

According to Eq.(10)-(11), the intrinsic time scale of intensity decay from the initial condition is determined by the boundary layer depth scale h and the steady-state final intensity v_f , taking C_k as constant, such that a smaller h leads to a faster decay (Fig.1b). Effects from changes in the external environment, e.g., surface properties, are captured in the prediction of v_f as discussed below. Notably, the precise definition of h in E12 theory and its relation to the true boundary layer height, H , is uncertain both theoretically and practically. First and foremost, the TC boundary layer height H is poorly understood even for storms over the ocean where the H is approximated by its dynamical or thermodynamical characteristics (Kepert 2001; Emanuel 1997; Bryan and Rotunno 2009; Zhang et al. 2011; Seidel et al. 2010). Unfortunately, these estimates of boundary layer heights can vary substantially from one another (Zhang et al. 2011). Moreover, in E12 theory it is the boundary layer depth specifically within the deeply-convecting eyewall that is relevant, where air rapidly rising out of the boundary layer effectively blurs the distinction between boundary layer and free troposphere (Marks et al. 2008; Kepert 2010; Smith and Montgomery 2010); perhaps for this reason E12 found a value corresponding to an approximate half-depth of the troposphere (5km) to perform best. Finally, little is known about the TC boundary layer height during the landfall transition. Thus, when evaluating E12 theory, we simply test a range of values for h and examine the extent to which variations in the best-fit values of h across experiments align with variations in estimates of the boundary layer.

3. Methodology

Idealized numerical simulation experiments of landfall are used to test the theoretical predictions discussed above.

a. Simulation setup

The pronounced spatiotemporal heterogeneity in surface properties from storm to storm in real-world landfalls

TABLE 1. Parameter values of the CTRL simulation.

Model	Name	Value
l_h	hor. mixing length	750-m
l_{inf}	asymptotic ver. mixing length	100-m
C_k	exchange coef. of enthalpy	0.0015
C_d	exchange coef. of momentum	0.0015
H_{domain}	model height	25-km
L_{domain}	model radius	3000-km
Environment	Name	Value
T_{ST}	surface temperature	300-K
T_{pp}	tropopause temperature	200-K
Q_{cool}	radiative cooling (θ)	1 K day^{-1}
f	Coriolis Parameter	$5 \times 10^{-5} \text{ s}^{-1}$

requires sophisticated land-surface and boundary layer parameterizations (Cosby et al. 1984; Stull 1988; Davis et al. 2008; Nolan et al. 2009; Jin et al. 2010). However, experiments in axisymmetric geometry with a uniform environment and boundary forcing can reveal the fundamental responses of a mature TC to individual surface roughening or drying, as introduced in CC20. Thus, this work extends the individual forcing experiments of CC20 to simulations where the surface is simultaneously dried and roughened with varying magnitudes of each.

All experiments are performed using the Bryan Cloud Model (CM1v19.8) (Bryan and Fritsch 2002) in axisymmetric geometry with same setup as Chen and Chavas (2020); model parameters are summarized in Table 1. Dissipative heating is included. We first run a 200-day baseline experiment to allow a mature storm to reach a statistical steady-state, from which we identify the most stable 15-day period. We then define the Control experiment (CTRL) as the ensemble-mean of five 10-day segments of the baseline experiment from this stable period whose start times are each one day apart. From each of the five CTRL ensemble member start times, we perform idealized landfall restart experiments by instantaneously modifying the surface wetness and/or roughness beneath the CTRL TC, which are then averaged into experimental ensembles analogous to the CTRL. Surface wetness is modified by decreasing the surface evaporative fraction ε , which reduces the surface latent heat fluxes F_{LH} through the decreased surface mixing ratio fluxes F_{qv} in CM1 (sfcpys.F) as

$$F_{qv} = \varepsilon s_{10} C_q \Delta q \quad (12)$$

$$F_{LH} = \rho L_v F_{qv} \quad (13)$$

where C_q is the exchange coefficients for the surface moisture; s_{10} is the 10-m wind speed; and Δq is the moisture disequilibrium between the 10-m layer and the sea surface. Surface roughness is modified by increasing the drag coefficient C_d , which modulates the surface roughness length

CTRL ($\tilde{V}_p = 1$)	0.7 ϵ (0.84)	0.5 ϵ (0.72)	0.3 ϵ (0.57)	0.25 ϵ (0.52)	0.1 ϵ (0.36)	No Surface Heat Fluxes (0)
2 C_d (0.71)	0.7 ϵ 2 C_d	0.5 ϵ 2 C_d	0.3 ϵ 2 C_d	0.25 ϵ 2 C_d	0.1 ϵ 2 C_d	0 V_p 2 C_d
4 C_d (0.5)	0.7 ϵ 4 C_d	0.5 ϵ 4 C_d	0.3 ϵ 4 C_d	0.25 ϵ 4 C_d	0.1 ϵ 4 C_d	0 V_p 4 C_d
6 C_d (0.41)	0.7 ϵ 6 C_d	0.5 ϵ 6 C_d	0.3 ϵ 6 C_d	0.25 ϵ 6 C_d	0.1 ϵ 6 C_d	0 V_p 6 C_d
8 C_d (0.353)	0.7 ϵ 8 C_d	0.5 ϵ 8 C_d	0.3 ϵ 8 C_d	0.25 ϵ 8 C_d	0.1 ϵ 8 C_d	0 V_p 8 C_d
10 C_d (0.316)	0.7 ϵ 10 C_d	0.5 ϵ 10 C_d	0.3 ϵ 10 C_d	0.25 ϵ 10 C_d	0.1 ϵ 10 C_d	0 V_p 10 C_d

Reduce the ϵ : surface drying \rightarrow

Increase the C_d :
surface roughening \downarrow

FIG. 2. Two-dimensional experimental phase space of surface drying (decreasing ϵ moving left to right) and surface roughening (increasing C_d moving top to bottom). CTRL is an ocean-like surface with $(C_d, \epsilon) = (0.0015, 1)$. Values of the potential intensity response \tilde{V}_p for CTRL and individual drying or roughening are listed in parentheses; \tilde{V}_p for any combination of forcing is the product of \tilde{V}_p for each individual forcing. Experiments testing combined forcings are shaded grey and the subset testing the most extreme combinations of each forcing are underlined. Experiment set $0V_pXC_d$, corresponding to the special case where surface heat fluxes are entirely removed ($V_p = 0$), are shaded green.

z_0 and in turn the friction velocity u^* for the surface log-layer in CM1 as

$$z_0 = \frac{z}{e^{\left(\frac{\kappa}{\sqrt{c_d}} - 1\right)}} \quad (14)$$

$$u^* = \max \left[\frac{\kappa s_1}{\ln \left(\frac{z_a}{z_0} + 1 \right)}, 1.0^{-6} \right] \quad (15)$$

where κ is the von Kármán constant, $z = 10m$ is the reference height, s_1 is the total wind speed on the lowest model, and z_a is approximately equal to the lowest model level height. Readers are referred to CC20 for full details.

Our experiments are summarized in Fig.2. Surface roughening-only experiments (2 C_d , 4 C_d , 6 C_d , 8 C_d , 10 C_d) and drying-only experiments (0.7 ϵ , 0.5 ϵ , 0.3 ϵ , 0.25 ϵ , 0.1 ϵ) are fully introduced in CC20. The combined experiments are simulated in the same manner but with the surface dried and roughened simultaneously. Our combined experiments are designed in a way where individual drying and roughening are systematically paired with each other; experiments are named by the corresponding modifications in C_d and ϵ . We focus on two specific subsets of experiments within this phase space. First, 0.7 ϵ 2 C_d , 0.7 ϵ 10 C_d , 0.1 ϵ 2 C_d , 0.1 ϵ 10 C_d are chosen as the representatives for extreme combinations, where each forcing takes its highest or lowest non-zero magnitude. Second, 0.25 ϵ 4 C_d , 0.5 ϵ 2 C_d , 0.1 ϵ 8 C_d are chosen to represent cases where the individual forcings are varied in ways that yield comparable equilibrium potential intensities; $\tilde{V}_{p(\epsilon)}$ and

$\tilde{V}_{p(C_d)}$ are labeled in Figure 2. Finally, we generate a special set of combined experiments, $0V_pXC_d$, in which \tilde{V}_p is fully reduced to zero for a range of magnitudes of roughening. Experiments are modeled by setting both surface sensible and latent heat fluxes to zero while increasing the roughness by a factor of X . This set of experiments sharing the same $\tilde{V}_p = 0$ and are applied to test the simplified form of E12 assuming $\tilde{v}_f = 0$ (Eq.(11)).

b. Testing theory against simulations

In each experiment, the simulated storm intensity $v_m(\tau)$ is normalized by the time-dependent, quasi-stable CTRL value, where τ denotes the time since the start of a given forcing experiment. We primarily focus on the first 36-h evolution, during which \tilde{v}_m decreases monotonically across all roughening, drying, and combined experiments. In addition, both the near-surface (50m) intensity response $\tilde{v}_{m(50m)}$ and above-BL (2km) intensity response $\tilde{v}_{m(2km)}$ are compared to theoretical predictions. The near-surface wind field is essential for predicting the inland TC hazards, while the above-BL wind field is generally used when formulating physically-based theories above the boundary layer. Over the ocean, $\tilde{v}_{m(50m)}$ and $\tilde{v}_{m(2km)}$ typically co-evolve closely (Powell et al. 2003). However, at and after landfall, the response of near-surface winds is expected to deviate from the above-BL winds, particularly in the case of roughening, as shown in CC20: there is a very rapid initial response of angular momentum to enhanced friction near the surface during the first 10 minutes (and especially the first 5-6 minutes) that subsequently propagates upward as the vortex decays. In contrast, the response to surface drying initially occurs aloft in the eyewall before propagating into the boundary layer, though this response is generally slower and smoother in time. Therefore, it is practically useful to test intensity theories against both near-surface and above-BL winds.

For E86 theory, we first compare the simulated equilibrium intensity against the equilibrium E86 prediction of Eq.(6). We then compare the full time-dependent simulated intensity response against that predicted by assuming the total response is the product of the individual responses, $\tilde{v}^*(\tau)$ (Eq.(8)). For E12 theory, we compare the simulated intensity evolution $\tilde{v}_m(\tau)$ against the E12 prediction $\tilde{v}_{m(th)}(\tau)$ of Eq.(10)-Eq.(11). In these solutions, the initial intensity $v_m(0) = 100.4ms^{-1}$ for 2km wind field and $v_m(0) = 90.38ms^{-1}$ for 50m wind field, respectively. The final intensity v_f is set as the minimum value of v_m in each simulation during the evolution. A range of h will be tested in Eq.(10), which will be discussed in the following subsection. For real-world landfalls, we do not know the minimum intensity prior to the inland evolution. Thus, as a final step, we compare simulation results against the theory with \tilde{v}_f predicted from \tilde{V}_p . This final step may be use-

ful for potentially applying the theory to real-world landfalls.

c. The boundary layer depth scale h

As introduced in Section 2, h is an uncertain boundary layer height scale both theoretically, as it is assumed to be constant, and in practice, because we do not have a simple means of defining the boundary layer depth particularly during the landfall transition. Thus, we do not aim to resolve this uncertainty in h in the context of landfall, but rather we simply test what values of h provide the best predictions and evaluate to what extent variations in h across experiments align with variations in estimates of the boundary layer height H .

For each simulation, we test a range of constant values of h from 1.0 to 6.0 km in 0.1 km increments in order to identify a best-fit boundary layer depth scale, h_{BEST} . We define h_{BEST} as the value of h that produces the smallest average error throughout the first 36-h evolution for each experiment. We then compare the systematic variation in h_{BEST} against that of three typical estimates of boundary layer height H calculated from each simulation.

Since the E12 solution applies within the convecting eyewall region, we estimate H using three typical approximations and measure the value at the radius of maximum wind speed (r_{max}) at the lowest model level: 1. H_{v_m} is the height of maximum tangential wind speed (Bryan and Rotunno 2009); 2. H_{inflow} is the height where radial wind u in the eyewall first decreases to 10% of its surface value (Zhang et al. 2011); and 3. H_{θ_v} is defined as the height where θ_v in the eyewall matches its value at the lowest model level (Seidel et al. 2010). The 36-h evolution of each estimate of H across our simulations is shown in Supplementary Figure 1. Considering that H varies in time during the experiment, the averaged value of H during $\tau = 0 - 6 h$ and $\tau = 30 - 36 h$ are each compared to the h_{BEST} .

4. Results

a. Near-surface vs. above-BL intensity response

As discussed in Section 3b, the simulated intensity responses near the surface ($z = 50m$) and above the boundary layer ($z = 2km$) may differ, and thus we intend to test the theory against both. We begin by simply identifying important differences between the intensity responses at each level.

For drying-only experiments, $\tilde{v}_{m(2km)}$ responds to reduced ε before $\tilde{v}_{m(50m)}$ during the initial ~ 5 hours (Fig.3a), where stronger drying results in a larger deviation between the responses at each level. $\tilde{v}_{m(2km)}$ decreases slightly more rapidly than $\tilde{v}_{m(50m)}$ but they eventually converge to comparable equilibria. In contrast, for roughening $\tilde{v}_{m(50m)}$ responds nearly instantaneously across all

roughening experiments, whereas $\tilde{v}_{m(2km)}$ responds more gradually. The magnitude of the deviation of $\tilde{v}_{m(50m)}$ from $\tilde{v}_{m(2km)}$ during the first 20 hours increases with increasing roughening (Fig.3b), though again both converge to comparable values after $\tau = 20 h$. The above behavior is consistent with the findings in CC20, where surface roughening has a significant and immediate impact on near-surface intensity while drying first impacts the eyewall aloft. As noted in CC20, \tilde{V}_p provides a reasonable prediction for the long-term equilibrium intensity response to each individual forcing; there is a small overshoot in roughening experiments where \tilde{v}_m reaches a minimum that is less than \tilde{V}_p at approximately $\tau = 36 h$ before increasingly gradually towards \tilde{V}_p .

For our combined experiment sets (Fig.3c-d), both surface drying and roughening determine the total response of storm intensity. However, regardless of the relative strength of each forcing, $\tilde{v}_{m(50m)}$ always decreases more rapidly than $\tilde{v}_{m(2km)}$ due to the surface roughening. Similar to the roughening-only experiment, stronger roughening results in a larger deviation of $\tilde{v}_{m(50m)}$ from $\tilde{v}_{m(2km)}$ during the first 20 hours. Overall, the rapid initial response of near-surface intensity is controlled by the surface roughening regardless of the surface drying magnitudes. Moreover, similar to the individual forcing experiments, \tilde{V}_p provides a reasonable prediction for the simulated minimum \tilde{v}_m in combined experiments used to define the theoretical final intensity \tilde{v}_f .

b. Deconstructing simultaneous drying and roughening

Now we focus on the full time-dependent responses of the combined forcing experiments. As noted above, we hypothesized based on traditional potential intensity theory (Eq.(5)-(7)) that the transient response of storm intensity to simultaneous drying and roughening can be predicted as the product of their individual responses (Eq.(8)). Thus, we compare the $\tilde{v}^*(\tau)$ to the simulated $\tilde{v}_m(\tau)$ of near-surface winds for each combined experiment (Fig.4) for our experiment set with extreme cases of combined drying and roughening. Regardless of the magnitude of roughening and/or drying, $\tilde{v}^*(\tau)$ follows the simulated $\tilde{v}_m(\tau)$ closely through the initial rapid decay forced by roughening, the weakening stage through 36 hours, and the final equilibrium stage. There is a slight low bias in $\tilde{v}^*(\tau)$ relative to the $\tilde{v}_m(\tau)$ throughout the primary weakening stage, especially for strong drying (Fig.4c-d), indicating that there is a slight compensation in the response to roughening when strong drying is also applied. Overall, though, the full temporal evolution of the normalized responses to drying and roughening can indeed be combined multiplicatively. A very similar result is obtained for the above-BL intensity as well (not shown).

Although E86 theory is formulated for the equilibrium intensity, the above results indicate that the implication

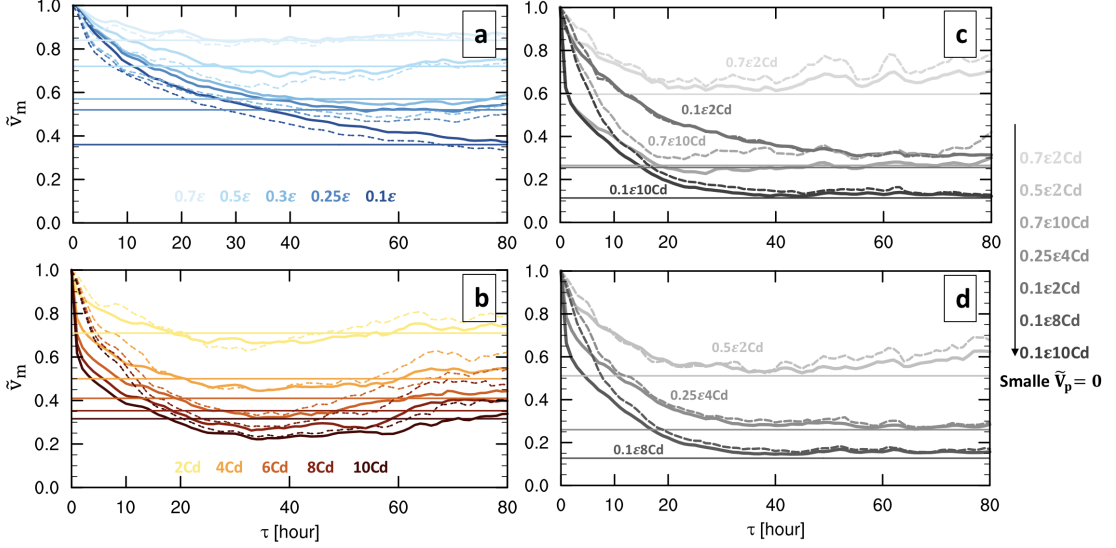


FIG. 3. Temporal evolution of simulated near-surface (50m, solid curves) and above-BL (2km, dash curves) \tilde{v}_m , across experiments: (a) surface drying, (b) surface roughening and (c)-(d) representative combined experiments. Potential intensity response, \tilde{V}_p (Eq.(4)-(6)), denoted by horizontal line. Darker color indicates a smaller \tilde{V}_p .

of its underlying physics also extends to the transient response to simultaneous surface drying and roughening. This behavior aligns with the notion that periods of intensity change represent a non-linear transition of the TC system between two equilibrium stable attractors given by the pre-forcing and post-forcing V_p (Kieu and Moon 2016; Kieu and Wang 2017). Because the distance between attractors is multiplicative, evidently so too is the trajectory between them.

c. Testing theory for transient intensity response

We next test the extent to which E12 theory (Eq.(10) and Eq.(11)) can predict the intensity evolution, taking as input \tilde{v}_f and a best-fit value of h_{BEST} from each simulation. The subsequent subsection compares the systematic variation in h_{BEST} against that of the estimated H in each set of experiments.

We begin by focusing on the above-BL intensity. The E12-based solution (Eq. (10)) can reasonably capture the overall transient intensity response across all roughening, drying, and combined experiments (Fig.5a-c). For drying-only experiments (Fig.5a), the theory initially ($\tau < 5$ h) underestimates $\tilde{v}_{m(2km)}$ (Fig.3a). h_{BEST} in drying experiments takes a value around 5 km and shows little systematic variations with increased drying magnitude (Fig.5a). In contrast, h_{BEST} decreases with increased surface roughening, from 4.3 km to 2.1 km (Fig.5b). In the following subsection, we compare this variation in h_{BEST} to that of multiple estimates of H .

For near-surface winds, E12 theory can capture the transient response of \tilde{v}_m in drying experiments (Fig.5d) using a slightly larger h_{BEST} . For roughening and combined experiments, though, it misses the very rapid initial decay due to enhanced C_d (Fig.3b-d and Fig.5e-f), which was shown in Fig.1 of CC20 to occur within the first 10 minutes. The magnitude of this rapid initial decay depends on C_d , as surface roughening immediately acts to rapidly remove momentum near the surface first. To account for this initial response, we propose a simple model for this initial decay of $\tilde{v}_{m(50m)}$ that may be derived from the tangential momentum equation in a 1D slab boundary layer with a depth of h^* , given by

$$h^* \frac{dv}{dt} = -C_d |\mathbf{v}| v \quad (16)$$

Taking $|\mathbf{v}| \approx v$, this equation may be integrated and then normalized by an initial intensity $v_m(0)$ to yield

$$\tilde{v}_{m(th)}(\tau) = \left(\frac{C_d v_m(0)}{h^*} \tau + 1 \right)^{-1} \quad (17)$$

Curiously, Eq.(17) is mathematically identical to the E12 solution with $v_f = 0$ (Eq.(11)) except with C_k replaced by $2C_d$, a topic we return to in the summary section.

We may combine Eq.(17) for the first 10-min evolution with Eq.(10) to model the complete near-surface intensity

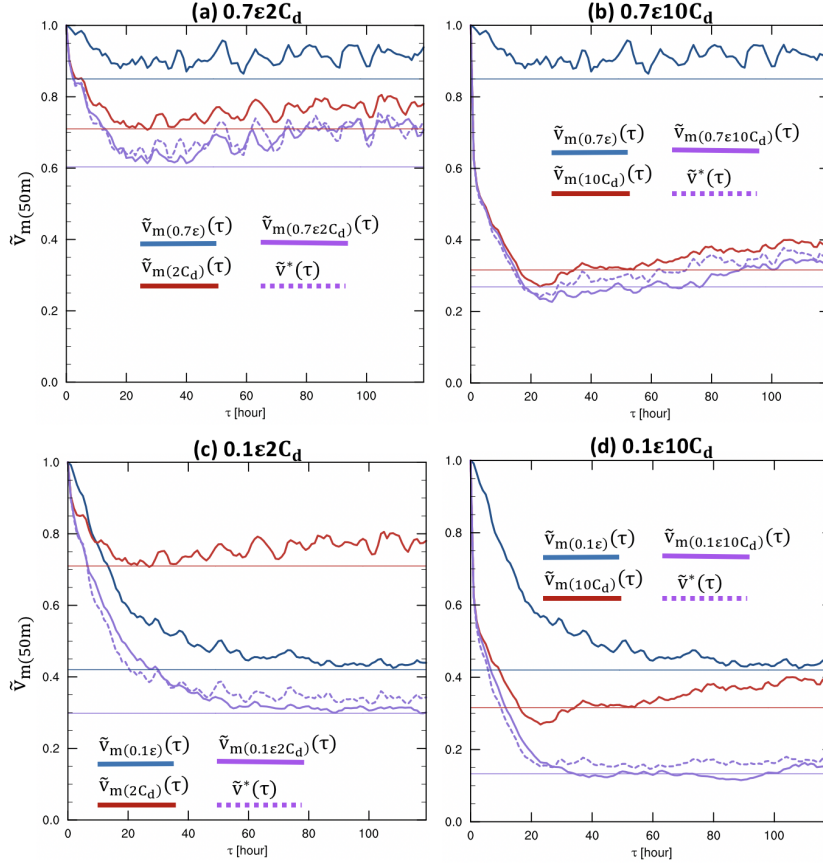


FIG. 4. Temporal evolution of simulated $\tilde{v}_m(\tau)$ for four representative combined experiments (solid purple) and their associated individual forcing experiments (solid blue for drying, solid red for roughening), with prediction $\tilde{v}^*(\tau)$ (dash purple; Eq.(8)) defined as the product of the individual forcing responses. Horizontal line denotes \tilde{V}_p , colored by experiment.

response to surface roughening:

$$\tilde{v}_{m(th)}(\tau) = \begin{cases} \left(\frac{C_d v_m(0)}{h^*} \tau + 1 \right)^{-1} & \tau \leq 10 \text{ min} \\ \tilde{v}_f \coth \left(\frac{C_k v_f}{2h} \tau + \tanh^{-1}(\tilde{v}_f^*) \right) & \tau > 10 \text{ min} \end{cases} \quad (18)$$

where $\tilde{v}_f^* = \frac{v_f}{v_{m(th)}(10 \text{ min})}$ since $v_{m(th)}$ now decreases from a new initial intensity $v_{m(th)}(10 \text{ min})$ calculated from the first equation. For the $\tau \leq 10 \text{ min}$ solution, we find that the rapid decay by $\tau = 10 \text{ min}$ across all roughening experiments can be captured by setting $h^* = 1.78 \text{ km}$ constant, which yields a constant decay rate during the period $\tau = 0 - 10 \text{ min}$. In reality, the decay rate is very large in the first minute and monotonically decreases through the 10 minute period. This time-varying decay rate can be reproduced by allowing h^* to increase with time from an initial very small value, which aligns with the physical response to roughening that may be thought of as the formation of a new internal boundary layer that begins at the surface and rapidly expands upward. Here though we employ a constant h^* in order to retain a simple analytic

solution; the 10-minute period is short enough that the difference is likely not of practical significance. Thereafter, we estimate h_{BEST} for each simulation in the same manner as before.

The comparison of model against simulations is shown in Fig.5e-f. Eq.(18) can capture the simulated near-surface transient intensity response $\tilde{v}_m(\tau)$ across roughening and combined experiments. The values of h_{BEST} for the prediction of $\tilde{v}_{m(50m)}$ are similar to those obtained for the above-BL case but slightly smaller in magnitude (Fig.5b,e and c,f).

Similar behavior associated with roughening is found in experiments for the special case $v_f = 0$ (Fig.6). Thus, we again propose a two-stage model for $\tilde{v}_{m(50m)}$ given by

$$\tilde{v}_{m(th)}(\tau) = \begin{cases} \left(\frac{C_d v_m(0)}{h^*} \tau + 1 \right)^{-1} & \tau \leq 10 \text{ min} \\ \left(\frac{C_k v_m(0)}{2h} \tau + \frac{v_m(0)}{v_{m(th)}(10 \text{ min})} \right)^{-1} & \tau > 10 \text{ min} \end{cases} \quad (19)$$

The comparison of model against simulations is shown in Fig.6, where h_{BEST} exhibits a decreasing trend with en-

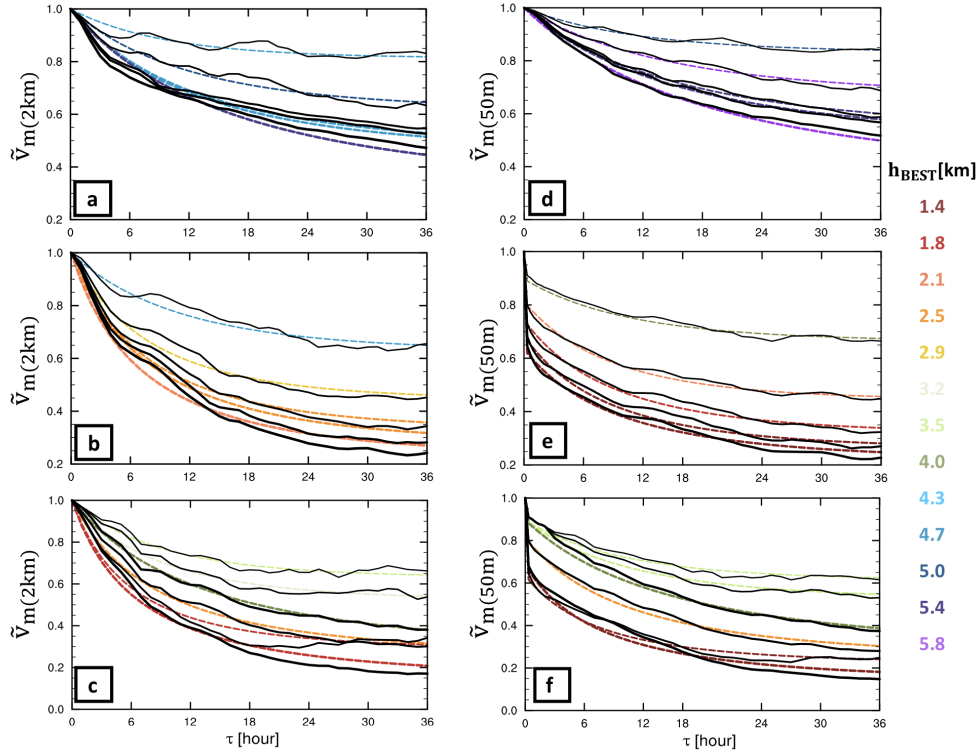


FIG. 5. (a-c) Temporal evolution of the simulated above-BL (2km) winds $\tilde{v}_m(\tau)$ (solid black) and theoretical prediction $\tilde{v}_{m(th)}(\tau)$ (dash colored; Eq.(10)) for (a) drying, (b) roughening and (c) combined experiments. $\tilde{v}_{m(th)}(\tau)$ is colored by the value of best-fit value of h , h_{BEST} . (d-f) are same as (a-c) but for the near-surface (50m) wind, in which (e-f) are the predictions from Eq.(18) to account for the initial rapid decay due to roughening.

hanced surface roughening, similar to that found in the pure roughening experiments.

Note that multiplying both sides of (17) by v yields a budget equation for kinetic energy given by $h \frac{d(KE)}{dt} = -C_d v^3$, where $KE = \frac{1}{2} v^2$ and the RHS is the expression for surface frictional dissipation of kinetic energy that is standard in TC theory (Bister and Emanuel 1998; Tang and Emanuel 2010; Chavas 2017)¹. Physically, then, the solution for the initial roughening response represents the intensity response to the dominant sink of kinetic energy in the absence of the dominant compensating thermodynamic source of kinetic energy from surface heat fluxes for a tropical cyclone. After this initial response, the solution follows a solution that accounts for both source and sink as encoded in E12 theory. The interpretation is that there exists a brief initial period where surface roughening directly modifies the near-surface air in a manner that is thermodynamically independent of the rest of the vortex. Thereafter, the vortex has adjusted and weakening proceeds according to processes governed by the full TC system, analogous to that of drying. In reality this transi-

tion is likely not instantaneous, though we have modeled it as so here for simplicity. The details of this adjustment process warrant more in-depth investigation that is left for future work.

1) COMPARING THE VARIATION OF h_{BEST} AND ESTIMATES OF H

We next compare the variations of h_{BEST} from our simulations to that of three common estimates of the boundary layer height: H_{v_m} , H_{inflow} , and H_{θ_v} . We compare trends for both the initial response (0-6h) and the equilibrium response (30-36h) (Fig.7d-f). As noted above, h_{BEST} was found to decrease with increased roughening (Fig.7a) but remain relatively constant for increased drying (Fig.7b). Moreover, h_{BEST} values are quite similar when estimated from the above-BL vs. near-surface responses (Fig.7a-c), and hence this discussion is not dependent on the choice of level for defining h_{BEST} .

To show the variation of estimates of H in different sets of experiments, we normalize each H by its corresponding value in the CTRL experiment as $\frac{H_{exp}}{H_{CTRL}}$ (Fig.7d-f), where each estimate of H in the CTRL experiment is quasi-stable (Supplementary Fig.1). We focus first on the

¹Note: the KE budget equation may be expressed as $h \frac{d(KE)}{dt} = -2C_d |v|(KE)$. Hence, $2C_d$ represents the surface exchange coefficient of kinetic energy over a static surface.

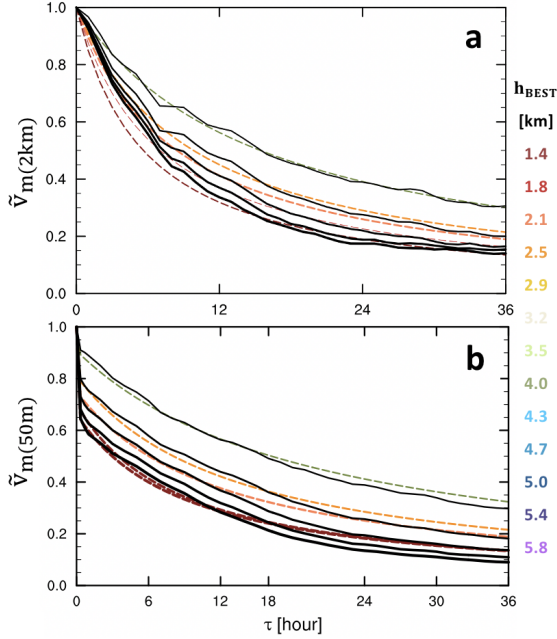


FIG. 6. Temporal evolution of simulated intensity response and theoretical prediction for the experiment set $0V_pXC_d$: (a) above-BL 2km winds (Eq.(11)) and (b) near-surface 50m winds (Eq.(19)). E12-based prediction is colored by the value of h_{BEST} for corresponding experiment.

responses to pure roughening or pure drying (Fig.7, top two rows). During 0-6h, all three estimates of H slightly increase with enhanced roughening and are approximately constant with enhanced drying (Fig.7d-f, color). By 30-36h, H decreases with enhanced roughening and enhanced drying for H_{v_m} and H_{inflow} , while H_{θ_v} remains relatively constant for each (Fig.7d-f, shaded).

Overall, there is no single estimated H whose systematic variation matches that of h_{BEST} (Fig.7). For roughening-only experiments, the initial response of all three estimates of H with enhanced roughening is opposite to that of h_{BEST} (Fig.7a,d), though the slow response of each H for two of the estimates does show a decrease with enhanced roughening (Fig.7d, shaded). For drying-only experiments, the initial response of H is either constant or very slowly decreasing with enhanced drying (Fig.7b,e), similar to h_{BEST} . However, the slow response of H_{v_m} and H_{inflow} decreases with enhanced drying in contrast to the nearly constant h_{BEST} , while the slow response of H_{θ_v} is again relatively constant (Fig.7e, shaded).

Finally, for $0V_pXC_d$ experiments (Fig.6), h_{BEST} exhibits a similar systematic response to enhanced surface roughening as the pure roughening experiments (Fig.7 a,c). Turning off all heat fluxes does not significantly alter the variation of h_{BEST} with roughening relative to the pure-roughening experiments; this behavior is also similar to

the pure drying experiments where h_{BEST} remains constant with enhanced drying. The systematic variation in h_{BEST} disagrees with both the early and the slow response of all three estimates of H (Fig.7 c,f).

Note that for the combined experiments, there is no clear evidence to link the decreasing trend in h_{BEST} (Fig.5c,f) to the change in each individual forcing. Thus, we elect not to speculate on the details of h_{BEST} and H for the combined experiments; instead, we explore a more practical theoretical prediction for combined forcing cases that applies h_{BEST} to drying and roughening experiments individually as shown in the next section.

The disagreement in the systematic trends both among estimates of H and between those estimates H and h_{BEST} motivates the need for more detailed studies on the TC boundary layer during and after the landfall in future work. In terms of E12 theory, though the solution can reproduce the decay evolution, it also likely oversimplifies the TC boundary layer, where a constant h cannot fully capture the time- and the radially-varying response of boundary layer height to landfall-like surface forcing. In terms of boundary layer theory, the optimal definition of boundary layer depth is itself uncertain. Meanwhile, without a comprehensive understanding of the TC boundary layer during the landfall, it is unclear if one particular definition of H , if any, might be most appropriate for E12 theory within the eyewall. Therefore, having a better estimation of h in the E12 solution and an improved understanding of boundary layer evolution during the landfall would help explain the differences in systematic variations between h and estimates of H .

d. Predicting the intensity response combining equilibrium and transient theory

We may combine all theoretical findings presented above to predict the near-surface intensity response to idealized landfalls for experiments combining drying and roughening. This represents the most complex of our experimental outcomes. We begin from the result of Eq.(8) and predict the intensity response to simultaneous surface drying and roughening as the product of their individual predicted intensity responses:

$$\tilde{v}_{th}(C_d\epsilon) \approx \tilde{v}_{th}^* = \tilde{v}_{th}(C_d)\tilde{v}_{th}(\epsilon) \quad (20)$$

where $\tilde{v}_{th}(\epsilon)$ is generated by Eq.(10) and $\tilde{v}_{th}(C_d)$ is generated by Eq.(18). When applying the transient solution for each individual forcing component, we use the previously-identified h_{BEST} from Fig.7a-b and predict the \tilde{v}_f using \tilde{V}_p given by Eq.(4)-(5). In principle, an empirical model for h_{BEST} for each individual forcing could be generated from our data since h_{BEST} is approximately constant with enhanced drying and monotonically decreasing with enhanced roughening. But given the uncertainties in h_{BEST}

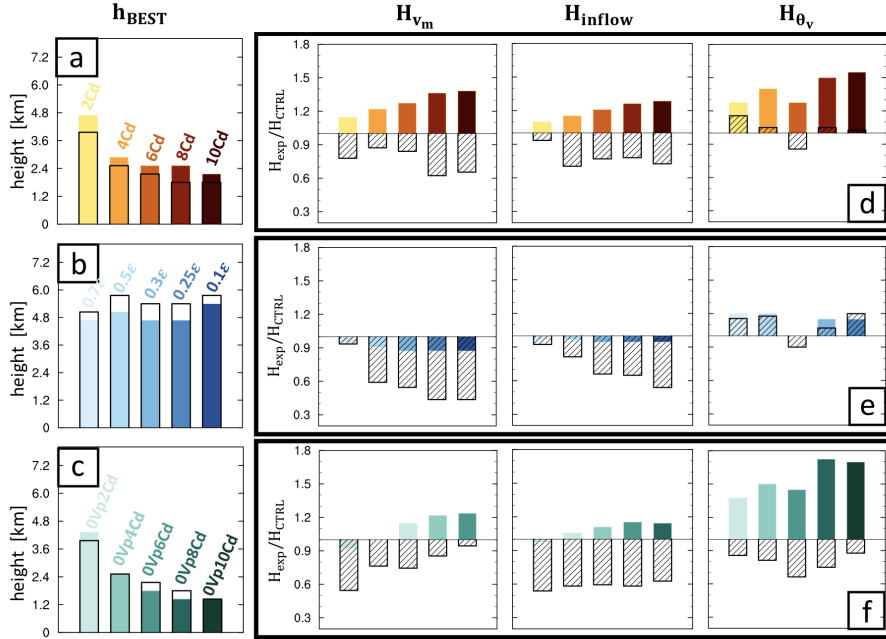


FIG. 7. Comparison of h_{BEST} (a-c) and the systematic variation of three estimates of boundary layer depth H (d-f) for each set of surface roughening, surface drying, and $0V_pXC_d$ experiments. For (a-c), h_{BEST} is shown for above-BL (color) and near-surface (box) intensity predictions. For (d-f), $\frac{H_{exp}}{H_{CTRL}}$ is shown for the early period ($\tau = 0 - 6h$; color) and later period ($\tau = 30 - 36h$; hatched box). The CTRL values of H_{v_m} , H_{inflow} , and H_{θ_v} are 0.95km, 1.56km, and 0.67km, respectively.

as a true physical parameter, we elect not to take such a step here.

The results are shown in Fig.8. Overall, our analytic theory performs well in capturing the first-order response across experiments, particularly given the relative simplicity of the method. There is a slight low bias in $\tilde{v}_{Th}(C_d\epsilon)$ (i.e., too strong of a response) across all the predictions relative to the simulations, a reflection of the slight compensation found in the assumption that the combined response may be modeled as the product of the individual responses in Fig.4. Therefore, knowing how each surface forcing is changed after landfall provides a theoretical time-dependent intensity response prediction when given estimates of \tilde{V}_p and h_{BEST} for any combination of uniform surface forcing. This offers an avenue to link our theoretical understanding to real-world landfalls.

e. Comparison with existing empirical decay model

Finally, as a first step toward linking theory and real-world landfalls, we provide a simple comparison of our theoretical model with the prevailing empirical model for inland decay. The model was first introduced by DeMaria and Kaplan (1995) and most recently applied to historical observations by Jing and Lin (2019) as

$$V(t) = V_b + (V_0 - V_b)e^{-\alpha t} \quad (21)$$

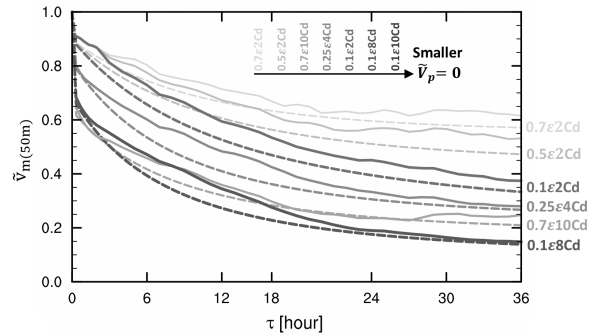


FIG. 8. Temporal evolution of simulated near-surface intensity response for combined forcing experiments (solid) and the corresponding prediction combining the equilibrium and transient theory (dash; Eq.(20)), with $\tilde{v}_f = \tilde{V}_p$ and setting h equal to the values of h_{BEST} for the individual predicted responses to drying (Eq.(10)) and roughening (Eq.(18)).

where storm landfall intensity V_0 decays to a background intensity V_b with a constant exponential decay rate α . Jing and Lin (2019) estimated $V_b = 18.82 \text{ kt}$ (9.7 ms^{-1}) and $\alpha = 0.049 \text{ h}^{-1}$ using the historical Atlantic hurricane database.

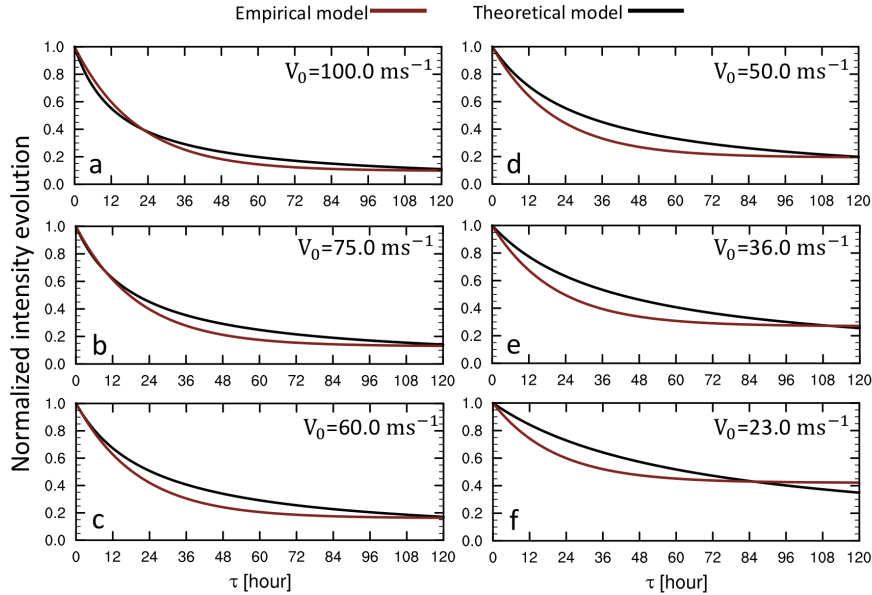


FIG. 9. Comparison between the theoretical intensity prediction for $v_f = 0$ (Eq.(11)) against the prevailing empirical exponential decay model prediction from Jing and Lin (2019) (Eq.(21)) for a range of initial intensities ([100, 75, 60, 50, 36, 23] ms^{-1}). For the theoretical prediction, $h=5\text{km}$.

Comparisons between theory and Eq.(21) predictions are shown in Fig.9, for V_0 from 100 ms^{-1} to 23 ms^{-1} similar to Jing and Lin (2019) (their Fig.3). Given that TCs in nature eventually dissipate (and typically do so rapidly), we choose the theoretical equation with $v_f = 0$ (Eq.(11)); this is also by far the simplest choice as no final intensity information is required. We set $h = 5\text{km}$ constant. Eq.(11) compares well against the empirical prediction for inland intensity decay, capturing the first-order structure of the characteristic response found in real-world storms. The comparison is poorer for weaker cases (Fig.9e-f), though uncertainties in intensity estimates are also likely highest for such weak storms. Note that the structure of the empirical model is constrained strongly by the assumption of an exponential model, so differences beyond the gross structure should not be overinterpreted. Ultimately, the consistency with the empirical model provides additional evidence that the physical model may indeed be applicable to the real world. Hence, it may help us to develop a physically-based understanding of the evolution of the TC after landfall.

5. Summary

This work tests the extent to which equilibrium and transient tropical cyclone intensity theory, the latter reformulated here to apply to inland intensity decay, can predict the simulated equilibrium and transient intensity response

of a mature tropical cyclone to surface drying, roughening, and their combination. This work builds off of the mechanistic study of Chen and Chavas (2020) that analyzed the responses of a mature tropical cyclone to these surface forcings applied individually. Key findings are as follows:

- The transient response of storm intensity to any combination of surface drying and roughening is well-captured as the product of the response to each forcing individually (Eq.(8)). That is, the time-dependent intensity evolution in response to a land-like surface can be understood and predicted via deconstructed physical processes caused by individual surface roughening and drying. Surface roughening imposes a strong and rapid initial response and hence dominates decay within the first few hours regardless of the magnitude of drying.
- The equilibrium response of storm intensity to simultaneous surface drying and roughening is well-predicted by traditional potential intensity theory (Eq.(6)).
- The transient response of storm intensity to drying and roughening can be predicted by the intensification theory of Emanuel (2012), which has been generalized to apply to weakening in this work (Eq.(10)). This theory predicts an intensity decay to a final, weaker equilibrium that can be estimated by Eq.(6).

The intensity prediction also depends on the boundary layer depth scale h , whose best-fit values are comparable to the value used in E12. Systematic trends of h to surface forcings do not clearly match commonly-defined TC boundary layer height.

- An additional modification is required to model the near-surface (50m) response specifically for surface roughening, which induces a rapid initial decay for near-surface intensity during the first 10 minutes. The magnitude of this initial rapid response increases with enhanced roughening and can be modeled analytically as a pure frictional spin-down (Eq.(17)-(18)).
- The above findings about the transient and equilibrium responses can be applied together to generate a theoretical prediction for the time-dependent intensity response to any combination of simultaneous surface drying and roughening (Eq.(20)). This prediction compares reasonably well against simulation experiments with both surface forcings.
- In the special case where the final equilibrium intensity is taken to be zero, the E12 solution reduces to a simpler analytic form that depends only on initial intensity and boundary layer depth (Eq.(11)). This solution is found to compare well against experiments with surface fluxes turned off for a range of magnitudes of surface roughening. It also compares well with the prevailing empirical model for landfall decay (Eq.(21)) across a range of initial intensities.

Although existing intensity theories are formulated for the tropical cyclone over the ocean, the above findings suggest that those underlying physics may also be valid in the post-landfall storm evolution. Note that we have not systematically tested the underlying assumptions of the theory but have focused on testing the performance of theories for predicting the response to idealized landfalls. The principal result is that for an idealized landfall, one can generate a reasonable prediction for the time-dependent intensity evolution if the inland surface properties along the TC track are known.

Landfall in the real world is certainly much more complicated. The real world has substantial horizontal variability in surface properties compared to the simplified idealized landfalls where only the surface roughness and wetness beneath the storm are instantaneously and uniformly modified. Additional environmental variability during the transition, including heterogeneity in surface temperature and moisture, environmental stratification, topography, land-atmosphere feedbacks, vertical wind shear, and translation speed, is excluded in these idealized simulations. Therefore, a theoretical prediction for the first-order intensity response to major post-landfall

surface forcings in an idealized setting provides a foundation for understanding TC landfall in nature. In this vein, our results suggest that the TC landfall process could plausibly be deconstructed into transient responses to individual surface and/or environmental forcings as encoded in our existing theories. One implication of this work is the potential to predict how post-landfall intensity decay may change in a changing climate if we know how each surface forcing will change in the future (Zeng and Zhang 2020). Theoretical solutions presented in this work could also benefit current risk models for hazard prediction.

In terms of theory, future work may seek to test the theory against simulations in three-dimensional and/or coupled models that include additional complexities. That said, several questions pertinent to axisymmetric geometry remain open here: do changes in surface sensible heat fluxes significantly alter the response to surface drying? How might changes in C_k , whose variation after landfall is not known, alter the results? How should one optimally define TC boundary layer height for the convective eye-wall region where boundary layer air rises rapidly into updrafts, both in general and in the context of the transition from ocean to land? How best can this be used to approximate the boundary layer depth scale h in the theoretical solution?

Notably, the solution for pure frictional spin-down (Eq.(17)) and the E12 solution for zero final intensity (Eq.(11)) have an identical mathematical form, with the lone difference being trading the parameter C_k for $2C_d$. These are simply the exchange coefficients for the dominant kinetic energy source (enthalpy fluxes) and sink (frictional dissipation) for the TC, respectively. Physically, we interpreted these two solutions as found in our work as a transition from a rapid response governed by pure frictional spin-down to a response governed by the reintroduction of the counterbalancing thermodynamic source of energy for the tropical cyclone as encoded in Emanuel (2012) theory (and similarly in traditional time-dependent Carnot-based theory). More generally, though, why should the large difference in the underlying physics of these two regimes manifest itself mathematically as a simple switch in exchange coefficients? This is curious.

Finally, future work may seek to test these theoretical predictions against observations accounting for variations in surface properties. Here we showed that our physically-based model appears at least broadly consistent with the prevailing empirical exponential decay model, suggesting that our model may provide an avenue for explaining variability in decay rates both spatially and temporally, including across climate states. For example, theory may be useful to understand how surface properties facilitate those rare TCs that do not weaken after the landfall (Evans et al. 2011; Andersen and Shepherd 2013). This would help us link physical understanding to real-world landfalls, which is important for improving the modeling of inland hazards.

Acknowledgments. The authors thank for all conversations and advice from Frank Marks, Jun Zhang, Xiaomin Chen on the hurricane boundary layer. The authors were supported by NSF grants 1826161 and 1945113. We also thank for all feedbacks and conversations related to this research during 101th AGU and AMS annual fall meetings.

APPENDIX

The E12-based decay solution is derived from Eq.17 of Emanuel (2012), given by

$$\frac{\partial v_m}{\partial \tau} = \frac{C_k}{2h} (v_f^2 - v_m^2) \quad (\text{A1})$$

where v_m is the initial intensity (maximum tangential wind speed) and v_f is defined as the theoretical steady-state maximum intensity. However, v_f need not be larger than the current intensity but rather may be generalized to any final quasi-steady intensity, larger or smaller. Integrating Eq.A1 yields:

$$\int \frac{1}{v_f^2 - v_m^2} dv_m = \int \frac{C_k}{2h} d\tau \quad (\text{A2})$$

$$\frac{\ln |v_m + v_f| - \ln |v_m - v_f|}{2v_f} = \frac{C_k}{2h} \tau + C \quad (\text{A3})$$

$$\frac{|v_m + v_f|}{|v_m - v_f|} = e^{(2\frac{C_k v_f}{2h} \tau + C)} \quad (\text{A4})$$

Ramsay et al. (2020) showed that for intensification where $v_m < v_f$, the solution is

$$\begin{aligned} v_{m(th)}(\tau) &= v_f \left(\frac{e^{(2\frac{C_k v_f}{2h} \tau + \coth^{-1}(\frac{v_f}{v_m(0)}))} - 1}{e^{(2\frac{C_k v_f}{2h} \tau + \coth^{-1}(\frac{v_f}{v_m(0)}))} + 1} \right) \\ &= v_f \tanh \left(\frac{C_k v_f}{2h} \tau + \coth^{-1} \left(\frac{v_f}{v_m(0)} \right) \right) \end{aligned} \quad (\text{A5})$$

Eq.A5 reduces to Eq.19 of Emanuel (2012) when $v_m(\tau = 0) = 0$, for which $\coth^{-1}(\frac{v_f}{0}) = 0$.

Alternatively, for decay where $v_f < v_m$, the solution is

$$\begin{aligned} v_{m(th)}(\tau) &= v_f \left(\frac{e^{(2\frac{C_k v_f}{2h} \tau + \tanh^{-1}(\frac{v_f}{v_m(0)})} + 1)}{e^{(2\frac{C_k v_f}{2h} \tau + \tanh^{-1}(\frac{v_f}{v_m(0)})} - 1)} \right) \\ &= v_f \coth \left(\frac{C_k v_f}{2h} \tau + \tanh^{-1} \left(\frac{v_f}{v_m(0)} \right) \right) \end{aligned} \quad (\text{A6})$$

Eq.A6 may be normalized by $v_m(0)$ to define the intensity response relative to the initial intensity.

References

- Andersen, T., and J. M. Shepherd, 2013: A global spatiotemporal analysis of inland tropical cyclone maintenance or intensification. *Int. J. Climatol.*, **34**, 391–402.
- Bhowmik, S. K. R., S. D. Kotal, and S. R. Kalsi, 2005: An empirical model for predicting the decay of tropical cyclone wind speed after landfall over the indian region. *J. Appl. Meteor.*, **44**(1), 179–185.
- Bister, M., and K. E. Emanuel, 1998: Dissipative heating and hurricane intensity. *Meteor. Atmos. Phys.*, **65**, 233–240.
- Bryan, G., and R. Rotunno, 2009: The maximum intensity of tropical cyclones in axisymmetric numerical model simulations. *Mon. Wea. Rev.*, **137**, 1170–1789.
- Bryan, G. H., and J. M. Fritsch, 2002: A benchmark simulation for moist nonhydrostatic numerical models. *Mon. Wea. Rev.*, **130**, 2918–2928.
- Chavas, D. R., 2017: A simple derivation of tropical cyclone ventilation theory and its application to capped surface entropy fluxes. *J. Atmos. Sci.*, **74**(0), 2989–2996.
- Chen, J., and D. R. Chavas, 2020: The transient responses of an axisymmetric tropical cyclone to instantaneous surface roughening and drying. *J. Atmos. Sci.*, **77**(8), 2807–2834.
- Cosby, B. J., G. Hornberger, R.B.Clapp, and T. Ginn, 1984: A statistical exploration of the relationships of soil moisture characteristics to the physical properties of soils. *Water Resources Research*, **20**(6), 682–690.
- Davis, C. A., and Coauthors, 2008: Prediction of landfalling hurricanes with the advanced hurricane wrf model. *Mon. Wea. Rev.*, **112**, 1990–2005.
- DeMaria, M., and J. Kaplan, 1994: Sea surface temperature and the maximum intensity of atlantic tropical cyclones. *J. Climate*, **7**, 1324–1334.
- DeMaria, M., and J. Kaplan, 1995: A simple empirical model for predicting the decay of tropical cyclone winds after landfall. *J. Appl. Meteor.*, **34**, 2499–2512.
- DeMaria, M., J. A. Knaff, and J. Kaplan, 2006: On the decay of tropical cyclone winds crossing narrow landmasses. *J. Appl. Meteor. Climatol.*, **45**, 491–499.
- DeMaria, M., M. Mainelli, L. K. Shay, J. A. Knaff, and J. Kaplan, 2005: Further improvements to the statistical hurricane intensity prediction scheme (ships). *Wea. Forecasting*, **20**, 531–543.
- Emanuel, K., S. Ravela, E. Vivant, and C. Risi, 2006: A statistical deterministic approach to hurricane risk assessment. *Bull. Amer. Meteor. Soc.*, **87**(3), 299–314.
- Emanuel, K. A., 1986: An air-sea interaction theory for tropical cyclones. part i: Steady-state maintenance. *J. Atmos. Sci.*, **43**, 585–605.
- Emanuel, K. A., 1997: Some aspects of hurricane innercore dynamics and energetics. *J. Atmos. Sci.*, **54**, 1014–1026.
- Emanuel, K. A., 2012: Self-stratification of tropical cyclone outflow: Part ii: Implications for storm intensification. *J. Atmos. Sci.*, **69**, 988–996.
- Emanuel, K. A., 2018: Corrigendum. *J. Atmos. Sci.*, **75**(6), 2155–2156.

- Emanuel, K. A., and R. Rotunno, 2011: Self-stratification of tropical cyclone outflow. part i: Implications for storm structure. *J. Atmos. Sci.*, **68**, 2236–2249.
- Evans, C., R. S. Schumacher, and T. J. Galarneau, 2011: Sensitivity in the overland reintensification of tropical cyclone erin (2007) to near-surface soil moisture characteristics. *Mon. Wea. Rev.*, **139**, 3848–3870.
- Jin, J., N. L. Miller, and N. Schlegel, 2010: Sensitivity study of four land surface schemes in the wrf model. *Adv. Meteor.*, 167436.
- Jing, R., and N. Lin, 2019: Tropical cyclone intensity evolution modeled as a dependent hidden markov process. *Journal of Climate*, **32(22)**, 7837–7855.
- Jing, R., and N. Lin, 2020: An environment-dependent probabilistic tropical cyclone model. *Adv. Model. Earth Syst.*, **12**, e2019MS00197.
- Kaplan, J., and M. DeMaria, 1995: A simple empirical model for predicting the decay of tropical cyclone winds after landfall. *J. Appl. Meteorol. Climatol.*, **34**, 2499–2512.
- Kaplan, J., and M. DeMaria, 2001: On the decay of tropical cyclone winds after landfall in the new england area. *Journal of Applied Meteorology*, **40(2)**, 280–286.
- Kepernt, J. D., 2001: The dynamics of boundary layer jets within the tropical cyclone core. part i: Linear theory. *J. Atmos. Sci.*, **58**, 2469–2484.
- Kepernt, J. D., 2010: Comparing slab and height-resolving models of the tropical cyclone boundary layer. part i: Comparing the simulations. *J. Quart. J. Roy. Meteor. Soc.*, **136(652)**, 1689–1699.
- Kieu, C., and Z. Moon, 2016: Hurricane intensity predictability. *Bull. Amer. Meteor. Soc.*, **90(10)**, 1847–1857.
- Kieu, C., and Q. Wang, 2017: Stability of the tropical cyclone intensity equilibrium. *J. Atmos. Sci.*, **74(11)**, 3591–3608.
- Knaff, J. A., C. Sampson, and M. DeMaria, 2005: An operational statistical typhoon intensity prediction scheme for the western north pacific. *Weather and Forecasting*, **20(4)**, 688–699.
- Kossin, J., 2018: A global slowdown of tropical-cyclone translation speed. *Nature*, **558**, 104–107.
- Kossin, J., 2019: Reply to: Moon, i.-j. et al.; lanzante, j. r. *Nature*, **570**, E16–E22.
- Li, L., and P. Chakraborty, 2020: Slower decay of landfalling hurricanes in a warming world. *Nature*, **587**, 230–234.
- Lilly, D. K., and K. Emanuel, 1985: A steady-state hurricane model. *16th Conf. on Hurricanes and Tropical Meteorology, Houston, TX, Amer. Meteor. Soc.*, 142–143.
- Liu, Y., D.-L. Zhang, and M. K. Yau, 2017: A multiscale numerical study of hurricane andrew (1992). part i: Explicit simulation and verification. *Mon. Wea. Rev.*, **125**, 3073–3093.
- Marks, F. D. J., P. Black, M. T. Montgomery, and et al., 2008: Structure of the eye and eyewall of hurricane hugo (1989). *Mon. Wea. Rev.*, **136(4)**, 1237–1259.
- Nolan, D., J. Zhang, and D. Stern, 2009: Evaluation of planetary boundary layer parameterizations in tropical cyclones by comparison of in-situ observations and high-resolution simulations of hurricane isabel (2003). part i: initialization, maximum winds, and the outer-core boundary layer. *Mon. Wea. Rev.*, **137**, 3651–3674.
- Powell, M. D., P. J. Vickery, and T. A. Reinhold, 2003: Reduced drag coefficient for high wind speeds in tropical cyclones. *Nature*, **422**, 279–283.
- Ramsay, H., M. Singh, and D. R. Chavas, 2020: Response of tropical cyclone formation and intensification rates to climate warming in idealized simulations. *J. Adv. Mod. Earth Syst.*, **12(0)**, e2020MS002086.
- Rappaport, E., 2000: Loss of life in the united states associated with recent atlantic tropical cyclones. *Bull. Amer. Meteor. Soc.*, **81**, 2065–2073.
- Rappaport, E., 2014: Fatalities in the united states from atlantic tropical cyclones: new data and interpretation. *Bull. Amer. Meteor. Soc.*, **95**, 341–346.
- Seidel, D. J., C. . Ao, and K. Li, 2010: Estimating climatological planetary boundary layer heights from radiosonde observations: Comparison of methods and uncertainty analysis. *Journal of Geophysical Research*, **115**, D16113.
- Shen, W., 2005: A simple prediction model of hurricane intensity. *Quart. J. Roy. Meteor. Soc.*, **131**, 2887–2906.
- Shutts, G. J., 1981: Hurricane structure and the zero potential vorticity approximation. *Mon. Wea. Rev.*, **109(2)**, 324–329.
- Smith, R. K., and M. T. Montgomery, 2010: Hurricane boundary-layer theory. *Quart. J. Roy. Meteor. Soc.*, **136A**, 1665–1670.
- Stull, R. B., 1988: Boundary layer conditions and surface forcings. *An Introduction to Boundary Layer Meteorology*, R. B. Stull, Ed., Kluwer Academic Pub, 261–270.
- Tang, B., and K. Emanuel, 2010: Midlevel ventilation’s constraint on tropical cyclone intensity. *J. Atmos. Sci.*, **67(6)**, 1817–1830.
- Vickery, P., P. F. Skerjil, and L. Twisdale, 2000: Simulation of hurricane risk in the u.s. using empirical track model. *ASCE J. Struct. Eng.*, **126**, 1222–1237.
- Vickery, P., and L. Twisdale, 1995: Wind-field and filling models for hurricane wind-speed prediction. *ASCE J. Struct. Eng.*, **121(11)**, 1700.
- Vickery, P. J., 2005: Simple empirical models for estimating the increase in the central pressure of tropical cyclones after landfall along the coast- line of the united states. *J. Appl. Meteorol.*, 1807–1826.
- Villarini, G., R. Goska, J. A. Smith, and G. A. Vecchi, 2014: North atlantic tropical cyclones and u.s. flooding. *Bull. Amer. Meteor. Soc.*, **95**, 1381–1388.
- Wong, M. L., J. C.-L. Chan, and W. Zhou, 2008: A simple empirical model for estimating the intensity change of tropical cyclones after landfall along the south china coast. *J. Appl. Meteor. Climatol.*, **47**, 326–338.
- Xi, D., N. N. Lin, and J. Smith, 2020: Evaluation of a physics-based tropical cyclone rainfall model for risk assessment. *Journal of Hydrometeorology*, **21(9)**, 2197–2218.
- Zeng, J., and Q. Zhang, 2020: The trends in land surface heat fluxes over global monsoon domains and their responses to monsoon and precipitation. *Sci Rep*, **10**, 5762.
- Zhang, J. A., R. F. Rogers, D. S. Nolan, and F. D. Marks, 2011: On the characteristic height scales of the hurricane boundary layer. *Mon. Wea. Rev.*, **139(8)**, 2523–2535.